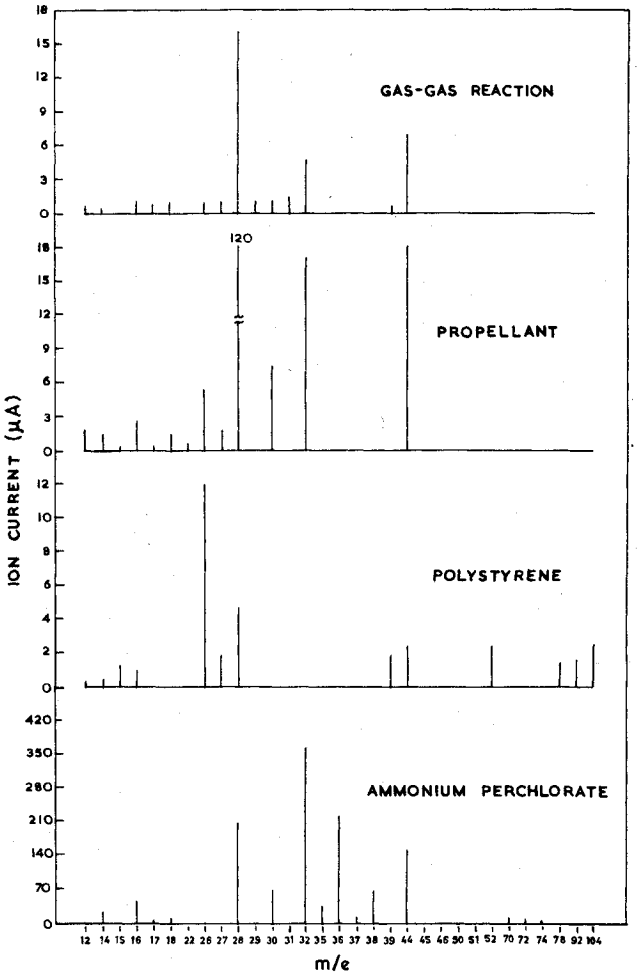

Fig. 2 Mass spectrum of ammonium perchlorate, polystyrene, propellant, and gas-gas reaction.

Results and Discussion

The mass spectra results are shown in Table 1. Although the related analysis of the mass numbers and hence of the products is under investigation, the data in its present form as shown in Table 1, clearly indicate that the propellant decomposition products are different from those of the decomposition products of their individual components. This can be seen better in Fig. 2 where the actual mass spectrograms for AP, PS, and the propellants are displayed.

This therefore suggests that the propellant decomposition is a nonadditive phenomenon. The decomposition products in experiments 1-3 are also different from the additive spectra of the individual spectra of PS and AP. Thus, even a physical mixture of AP and PS does not yield additive decomposition products of its components. This rules out our suspicion that the divergence of our data from that of Ref. 7 is due to the method of preparation. Therefore, the difference may be due to the lack of equilibrium in Ref. 7, which is probably due to the method in which sample was decomposed in MS chamber. A close inspection of our results at first glance suggests a similarity in the mass-spectral data of propellant (4) and gas-gas reaction (1) [see Fig. 2], which apparently supports the conclusion of Ref. 7. All the experimental runs (1-4) leave behind an yellow sublimate on the cooler part of the reaction vessel where the gases interact. Although detailed analysis of the products have not been yet completed, the preliminary analysis suggests that the yellow deposit is an aromatic compound containing chlorine. The presence of chlorine in yellow sublimate explains the mass spectra of propellant (4) and gas-gas reaction (1) in which chlorine peaks are absent. A point of interest here is the fact that although at 400°C the yellow compound is found as a sublimate, yet at 270°C on partial decomposition the entire-nondecomposed residue is intensely yellow-colored throughout the bulk of the solid residue, while no yellow sublimate is formed. On allowing the decomposition to go to completion at 270°C the yellow products, distributed uniformly throughout the bulk of propellant residue, sublimes on the cooler part of the vessel leaving behind a brown residue. This therefore suggests that the yellow compound is initially formed in the condensed phase

In conclusion, therefore, our results on the identification of the yellow compound in the bulk of propellant suggests a condensed phase reaction and the mass spectral results suggest that final products result from the interaction of the decomposition products of PS and AP individually. Experiments where AP and PS are allowed to decompose separately followed by an interaction of the products in the gas-phase compare favorably with the decomposition of the propellant as a whole thereby suggesting that the interaction of the product in the reaction vessel is similar to the interaction of AP and PS decomposition products in the porous matrix of the propellant. The occurrance of the reaction in the porous "Condensed Phase" of the propellant may explain the larger exothermicity of the propellant compared to the additive heats of decomposition of its components.[8]

References

[1]Sammons, G. D., "Study of the Thermal Behavior of Solid Propellants by Differential Scanning Calorimetry," *Analytical Calorimetry*, Pelnum Press, New York, 1968, pp. 305-311.

[2]Sammons, G. D., "Dynamic Calorimetric Solid-Propellant Combustion Studies," AIAA Paper 69-504, U.S. Air Force Academy, Colorado, 1969.

[3]Wenograd, J., "Study of the Kinetics and Energetics of Propellant Decomposition Reactions, and Application to Steady-State Combustion Mechanism," presented at the 3rd ICRPG Combustion Conference, CPIA Publication 138, Vol. I., Feb. 1967, p. 89.

[4]Hermance, C. E., "A Model of Composite Propellant Combustion Including Surface Heterogencity and Heat Generation," *AIAA Journal*, Vol. 4, Sept. 1966, pp. 1629-1637.

[5]Vantoch, P. and Parandjuk, S., "Solid Propellant Combustion," ATD Rept. 66-68, Aerospace Technology Division, Library of Congress, Aug. 1966.

[6]Selzer, H., "The Temperature Profile Beneath the Burning Surface of a Composite NH_4CLO_4 Propellant," *Proceedings of the 11th Symposium (International on Combustion)*, Combustion Institute, Pittsburg, Pa., 1966, pp. 439-446.

[7]Korobeinicha, O. P., Karpenko, Y. Y., and Boldyrev, V. V., "Study of Thermal Decomposition of Solid Fuels on the Basis of Ammonium Perchlorate and Polystyrene by Time of Flight Mass-Spectrometer," *Fig. Gor. Vzry*, Vol. 6, No. 2, 1970, pp. 248-250.

[8]Rastogi, R. P., Kishore, K. and Singh, G., "Solid Propellant Decomposition Studies by Differential Scanning Colorimetry," presented at the 29th Annual Calorimetry Conference, University of Tennesse, Knoxville, July 1974, *Thermochimica Acta*, Vol. 12, 1975, pp. 89-97.

[9]Rastogi, R. P., Kishore, K., and Singh, G., "Combustion of Polystyrene and Styrene-Oxygen Copolymer/NH_4C10_4 Propellants," *AIAA Journal*, Vol. 12, Jan. 1974, pp. 9-10.

Circular Elastic Membrane Loaded at Concentric Circle

Lars Lidin*
Volvo Flygmotor AB, Trollhättan, Sweden

Nomenclature

a = outer radius of membrane
E = Young's modulus
F = load at circle

Received February 27, 1975; revision received May 12, 1975.
Index category: Structural Static Analysis.
*Research Engineer.

f = nondimensional load
h = thickness of membrane
p = surface pressure
r = radial coordinate
s = nondimensional meridional stress
t = nondimensional circumferential stress
u = radial displacement
w = axial displacement
ϵ_r, ϵ_t = radial and circumferential strain
ν = Poisson's ratio
ξ = nondimensional radial displacement
ρ = nondimensional radius
σ_m, σ_t = meridional and circumferential stress
φ = slope of membrane

THE elastic membrane is a model approximating some real structures to a reasonable degree. A flat circular membrane with a load perpendicular to its surface thus approximates a thin plate. If the stiffness of the plate is also calculated by means of ordinary plate theory and the membrane and plate stiffnesses are added, a quite satisfactory solution is achieved. The membrane solution is straightforward for an evenly distributed load, as shown in textbooks such as that by den Hartog.[1]

This Note is concerned with the case of a load concentrated along a circle, concentric with the membrane. The corresponding plate stiffness can be found in Roark.[2] The present membrane solution is not an explicit formula, and it seems doubtful if one can be theoretically derived. Stress and deformation in a nondimensional form are given at a range of values for relevant parameters, however, and equations are given that yield a close approximation for the range studied.

A membrane is incapable, by definition, of sustaining point loads. The effect of a concentric line load at a circular membrane may be found as follows. The vertical equilibrium at any radius yields the equation

$$2\pi r h \sigma_m \sin\varphi = F \tag{1}$$

The equilibrium of the membrane further gives the general equation

$$(\sigma_m/R_m) + (\sigma_t/R_t) = (p/h) \tag{2}$$

The radii are immediately apparent in Fig. 1

$$R_m = (1+\varphi^2)^{3/2}/(d\varphi/dr); \quad R_t = r/\sin\varphi$$

If the surface load $p=0$ and the slope φ, in relevant cases, is small compared to unity, then Eq. (2) is transformed into

$$[\sigma_m(d\varphi/dr)] + [(\sigma_t/r)\sin\varphi] = 0 \tag{2a}$$

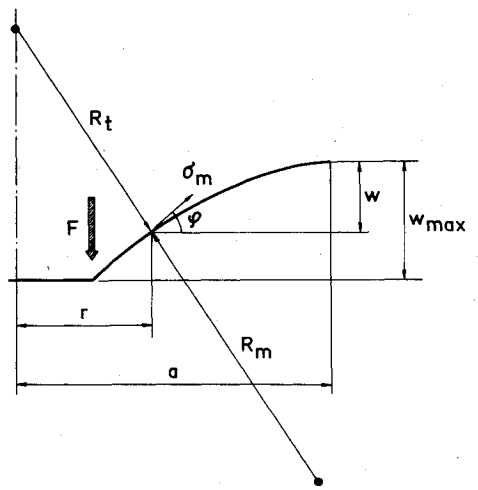

Fig. 1 Sketch of membrane.

With a radial displacement u, we can ascertain the radial and tangential strains

$$\epsilon_r = (du/dr) + \tfrac{1}{2}(dw/dr)^2$$

$$\epsilon_t = (u/r) \tag{2b}$$

and thus from Hooke's law

$$u = (r/E)\ (\sigma_t - \nu\,\sigma_m) \tag{3}$$

$$(du/dr) + \tfrac{1}{2}(dw/dr)^2 = (1/E)\ (\sigma_m - \nu\,\sigma_t) \tag{4}$$

Note that $dw/dr = \tan\varphi$. The boundary condition at the rim is conveniently expressed as $u=0$ at $r=a$. At the load radius r_l radial equilibrium yields the boundary condition

$$\sigma_{m\,II} = \sigma_{M\,I} \cdot \cos\varphi$$

The flat central part of the membrane is in a state of simple constant tension $\sigma_r = \sigma_t = \sigma_{m\,II}$ and thus from Hooke's law

$$\sigma_{m\Pi}(1-\nu) = E \cdot (u_l/r_l)$$

The differential equations and boundary conditions can be made nondimensional by the following substitutions:

$$u/r = \xi, \quad r/a = \rho, \quad r_l/a = \rho_l, \quad F/2\pi\, a\, E\, h = f,$$

$$\sigma_m/E = s, \quad \sigma_t/E = t$$

Note that

$$(du/dr) = \rho(d\xi/d\rho) + \xi$$

Thus we have

$$\rho\, s \sin\varphi = f \tag{5}$$

$$s(d\varphi/d\rho) + (t/\rho)\sin\varphi = 0 \tag{6}$$

$$\xi = t - \nu s \tag{7}$$

$$\rho(d\xi/d\rho) + \xi + [(\tan\varphi)^2/2] = s - \nu t \tag{8}$$

With boundary conditions

$$\xi = 0 \text{ at } \rho = 1$$

$$s\cos\varphi = \xi/(1-\nu) \text{ at } \rho = \rho_l$$

The following method of solution was employed. Take the first derivative with respect to ρ of Eq. (5)

$$\rho s \cos\varphi \frac{d\varphi}{d\rho} + \rho \frac{ds}{d\rho} \cdot \sin\varphi + s \sin\varphi = 0$$

giving

$$\frac{ds}{d\rho} \cdot \tan\varphi + s \frac{d\varphi}{d\rho} + \frac{s}{\rho}\tan\varphi = 0 \tag{5a}$$

Thus $d\varphi/d\rho$ is eliminated between Eq. (6) and (5a), giving

$$\frac{ds}{d\rho} = \frac{t\cos\varphi - s}{\rho} \tag{9}$$

Now take the derivative of Eq. (7)

$$\frac{d\xi}{d\rho} = \frac{dt}{d\rho} - \nu\frac{ds}{d\rho} \tag{7a}$$

Table 1 Nondimensional stress $s_{max} \times 10^4$ (at load)

ρ	0.9	0.8	0.7	0.6	0.5	0.4	0.3	0.2	0.1
$f \times 10^6$									
1	0.5435	0.7170	0.8671	1.021	1.198	1.423	1.748	2.309	3.678
2		1.138		1.621		2.259		3.665	
5		2.097		2.986		4.161		6.751	
10	2.524	3.328	4.025	4.740	5.560	6.606	8.116	10.72	17.08
20		5.284		7.524		10.49		17.02	
50		9.736		13.86		19.32		31.35	
100		15.46		22.01	25.82	30.68	37.70	49.79	
200		24.56		34.96		48.72		79.09	
500		45.29		64.45		89.85		145.9	

Table 2 Deformation under load $(w/a)_{max} \times 10^2$

ρ	0.9	0.8	0.7	0.6	0.5	0.4	0.3	0.2	0.1
$f \times 10^6$									
1	0.1964	0.3207	0.4331	0.5421	0.6519	0.7658	0.8876	1.023	1.183
2		0.4040		0.6830		0.9649		1.288	
5		0.5483		0.9269		1.310		1.749	
10	0.4230	0.6908	0.9330	1.168	1.404	1.650	1.912	2.203	2.549
20		0.8702		1.471		2.079		2.776	
50		1.181		1.997		2.821		3.767	
100		1.487		2.515	3.025	3.554	4.119	4.745	
200		1.873		3.168		4.477		5.978	
500		2.539		4.297		6.073		8.111	

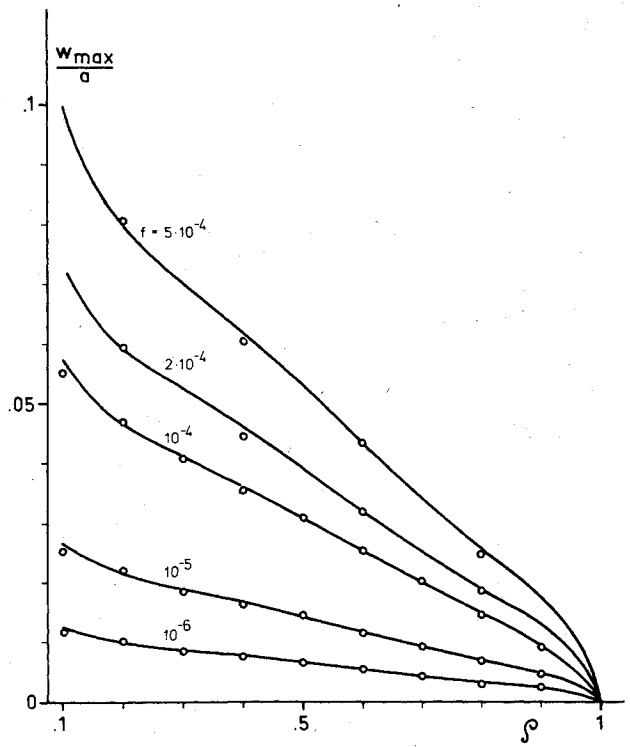

Fig. 2 Maximum deflection vs location of loading circle.

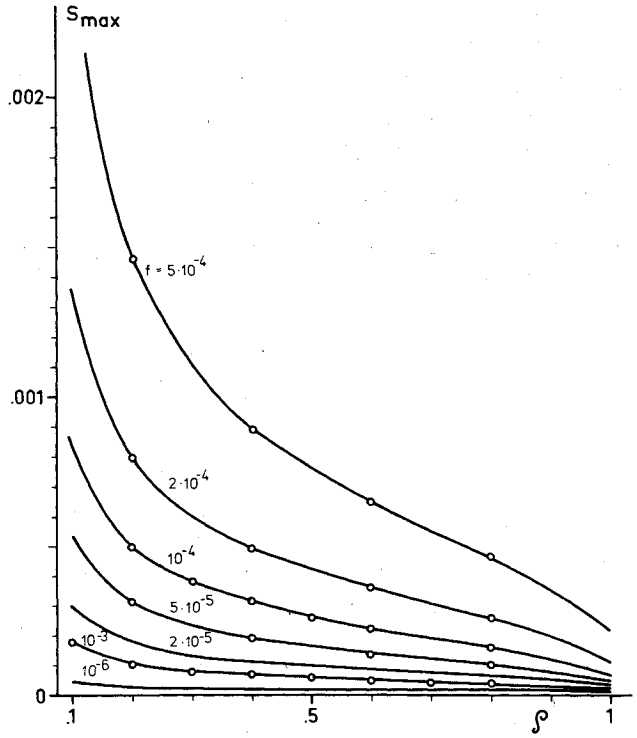

Fig. 3 Maximum stress vs location of loading circle.

Equations (7, 7a, and 9) reduce Eq. (8) into

$$\frac{dt}{d\rho} = [t\ \nu\cos\varphi - \nu s - t + \nu s - \tan^2\varphi/2 + s - \nu t]/\rho$$

$$= (s - t[1 - \nu(1-\cos\varphi)] - \tan^2\varphi/2)/\rho \qquad (10)$$

It is quite reasonable, for the range of values of interest, to assume $\cos\varphi \approx 1$, $\sin\varphi \approx \varphi$ and thus

$$\frac{ds}{d\rho} = \frac{t-s}{\rho} \qquad (9a)$$

$$\frac{dt}{d\rho} = (s - t - \varphi^2/2)/\rho \qquad (10a)$$

Now, for a certain value of the nondimensional load f and its radial location ρ_1, a slope φ_0 at $\rho = 1$ is assumed.

Then, from Eq. (5) and (7) and the boundary condition at $\rho = 1$, we have s and t at $\rho = 1$:

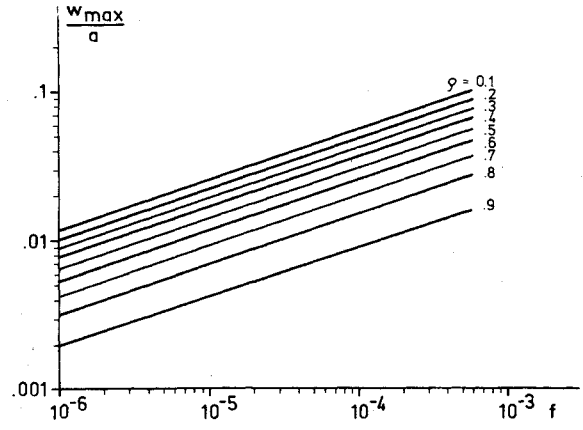

Fig. 4 Maximum deflection vs loading magnitude.

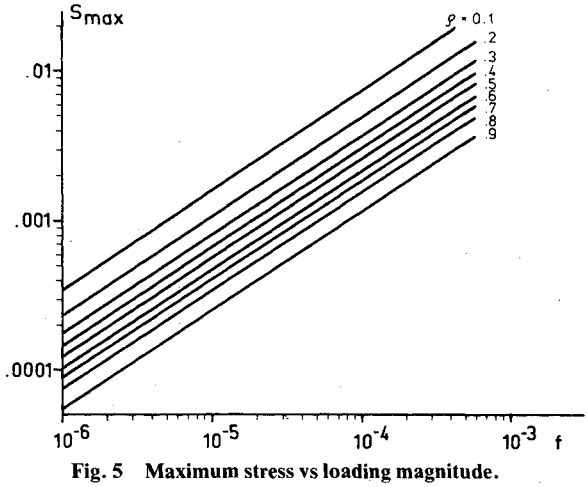

Fig. 5 Maximum stress vs loading magnitude.

$$s_0=(f/\rho\varphi_0) \qquad t_0=\nu\, s_0$$

By means of Eqs. (9a) and (10a), the nondimensional stresses s and t are then determined for radial locations between $\rho=1$ and $\rho=\rho_1$, and at the latter location, the boundary condition is checked. A corrected value of φ_0 is then chosen and the computation repeated until the correct boundary condition is obtained. This calculation has been carried out for a range of values of the parameters f and ρ_1, employing a Kutta-Merson procedure coded in APL, with a Burroughs computer (Table 1).

The necessary condition of small slope does not occur at small values of ρ_1. This is equivalent to approaching a point load which, as previously mentioned, cannot be carried by a membrane. Thus no calculations have been carried out for ρ_1 values below 0.1.

When s is determined, the slope φ is known from Eq. (5). The vertical displacement under the load can then be calculated by integrating the slope from the rim until the load radius (Table 2).

Maximum stress and deformation of the range $10^{-6}\leq 5\cdot 10^{-4}$ as thus calculated are shown in Figs. 2 and 3 by the points. The curves show the equations

$$\frac{w}{a}=f^{1/3}\cdot 0.158\left(\cot\frac{\pi}{1.1}\rho+0.94\sin\frac{\pi}{0.55}\rho+3.926\right)$$

$$s=f^{2/3}\cdot 0.862\left(1+0.8\cot\frac{\pi\rho}{1.41}\right)$$

These equations, which were evaluated as approximations for the result, thus appear to give quite a close coincidence. It should be noted that the proportionality to the powers ⅓ and ⅔ of f is in agreement with results for a distributed load.[1] As shown in Figs. 4 and 5, which give the same data as Figs. 2 and 3, the equations can, of course, be displayed as straight lines in a log-log diagram. The trigonometric functions, on the other hand, are just a trial-and-error fit, but apparently a successful one.

References

[1] den Hartog, J. P., *Advanced Strength of Materials*, McGraw-Hill, New York, 1952.

[2] Roark, R. J., *Formulas for Stress and Strain*, 4th ed., McGraw-Hill, New York, 1965.

Analytical Formulas for Conditions on Blunt Wedges in Hypersonic Flow

W. L. Bade*
Avco Systems Division, Wilmington, Mass.

Introduction

CHENG et al.[1] formulated an analytical theory of the combined effects of bluntness and boundary-layer displacement on the hypersonic flow over a wedge. Kemp[2] modified this analysis to include the effects of nonzero $(\lambda-)$ to first order. Boger and Aiello[3] generalized the theory to the case of nonzero yaw angle. The fundamental relation in the theory is the equation

$$(z-\Gamma\zeta)\frac{d}{d\zeta}\left(z\frac{dz}{d\zeta}\right)-\left(z\frac{dz}{d\zeta}\right)^{1/2}=1 \tag{1}$$

in which z is a nondimensional variable proportional to the shock ordinate, ζ a nondimensional distance from the leading edge of the wedge, and Γ a constant parameter proportional to the angle of attack.

The boundary condition on Eq. (1) is $z=0$ at $\zeta=0$. The equation is singular at the origin. Sufficiently near the origin, the square root term and the term containing Γ can be neglected, and the equation admits a power-law solution $z=A\,\zeta^n$ with $n=2/3$, $A=(9/2)^{1/3}$. The solution for larger J can be generalized by numerical integration starting from a point on this singular solution.

For zero angle of attack, Eq. (1) has the analytical solution $z=z_0(\lambda)$, $\zeta=\zeta(\lambda)$, where

$$z_0(\lambda)=2[\tfrac{1}{3}\lambda^{3/2}-\tfrac{1}{2}\lambda+\lambda^{1/2}-\ln(1+\lambda^{1/2})] \tag{2a}$$

$$\zeta(\lambda)=\tfrac{1}{3}(1+\lambda^{1/2})^4-\frac{22}{9}(1+\lambda^{1/2})^3+9(1+\lambda^{1/2})^2-\frac{46}{3}(1+\lambda^{1/2})+\frac{10}{3}\ln(1+\lambda^{1/2})-4\lambda^{1/2}\ln(1+\lambda^{1/2})+2[\ln(1+\lambda^{1/2})]^2+\frac{76}{9} \tag{2b}$$

in terms of a parameter λ defined by

$$\lambda\equiv z\,dz/d\zeta \tag{3}$$

Received February 3, 1975; revision received March 10, 1975. This work was supported by NASA, Lyndon B. Johnson Space Center, under contract NAS9-9744.

Index categories: Rarefield Flows; Supersonic and Hypersonic Flow.

*Principal Staff Scientist.